Department of Precision and Microsystems Engineering

Aerosol Direct Write characteristics and deposition methodology for functional SERS substrates

T. van Zee

Report no	: 2023.034
Coach	: S. Aghajani
Professor	: Dr. A. Hunt
Specialisation	: Mechatronic System Design
Type of report	: Master Thesis
Date	: 13 June 2023

TU Delft Delft University of Technology

Challenge the future

Abstract - **Surface-enhanced Raman spectroscopy (SERS) is a powerful non-destructive molecule identification technique. The technique is made viable by the enhancement of the Raman effect which is caused by metallic nanoparticle (MNP) structures. A fabrication method that can manufacture highly consistent SERS substrates is important. Aerosol Direct Write (ADW) is a promising method to achieve consistent SERS substrates. Previous research did not achieve reproducible substrates due to inconsistencies in particle deposition. To improve the quality of SERS substrates fabricated using ADW, key factors within the ADW setup contributing to the substrate quality are identified and analysed. A particle deposition model is created to analyse the impact of those key factors on the substrate quality and to analyse if different operating velocities of the moving stage can minimise the impact of those key factors. The deposition model results are validated by fabricating substrates using a range of operating velocities. It is found that the nozzle diameter has a linear correlation with the spot size. The particle generation is inconsistent and a dominant factor for the SERS substrate quality. The effect of the fluctuating particle generation rate can be minimised by multiple path coverages and higher operation velocities. It is found that the XYZ-stage in the used setup operates optimally between $1000\,\mu m\,s^{-1}$ and $2000\,\mu m\,s^{-1}$. The deposition model correctly showed that the particle generation rate is the dominant factor for the substrate quality and correctly predicted the ideal operating velocity of the XYZ-stage used in the setup. The model can be used in the future to find an ideal operating velocity and to look at the effects of stage movement characteristics and particle generation fluctuations in ADW setups. SERS measurements show that the SERS substrate fabricated at the ideal operating velocity performed more consistently than substrates fabricated at other velocities.**

1 Introduction

Surface-enhanced Raman Spectroscopy (SERS) is a non-destructive molecule identification method based on the enhancement of the Raman scattering signal caused by metallic nanostructures [1]. The nanoparticles can enhance the signal up to a factor of 10^{11} [1]. The enhancement effect is very sensitive to structural differences of these metallic nanostructure substrates [2]. SERS is used in various domains, such as identification of diseases and food contaminants [3, 4, 5, 6]. The use is mainly limited to laboratories but the implementation of SERS in microfluidic devices could enable continuous and on-site use [3]. A fabrication method that can manufacture highly consistent substrates is important to implement SERS in microfluidic devices where the number of molecules to detect is low due to small sample volumes.

There are different methods to fabricate SERS substrates. The methods can be divided into wet chemistry methods and dry methods. Wet chemistry methods immobilize metallic nanoparticles (MNPs) suspended in a colloid onto a substrate using an adhesive layer. These processes can take days, offer little control over the MNP structure, and have low throughput. Lithography and template methods where MNPs are evaporated on a substrate are examples of dry methods. They offer more control over the substrate structure but they are expensive and also have low throughput. Dry aerosol direct write (ADW) is a promising dry method to fabricate SERS substrates [7, 8]. This method is used in combination with the spark ablation method (SAM) to create MNPs in line [9]. The particles are then suspended in a gas and deposited on a silicon substrate. The deposition is done in a low vacuum to avoid contamination of the deposited structure and to increase the dimensionless Stokes number of the particles so they keep their trajectory towards the silicon substrate. The substrate is attached to a moving XYZ-stage to create lines of MNP structures.

Previously, Aghajani et al [7, 8, 10] achieved the detection of Rhodamine B molecules with SERS substrates manufactured using ADW. However reproducible SERS substrates were not achieved due to inconsistencies in particle deposition.

The goal of this study is to identify the key factors within the ADW setup that affect the line quality, to find the sensitivity of different operating velocities to these key factors, and to find an ideal deposition strategy that minimises SERS substrate inconsistencies. To achieve this, the factors deemed to have to biggest impact on substrate quality are selected. Subsequently, three experiments are performed to measure the behaviour of the selected key factors. A deposition model will be created to predict particle deposition. The model will use the measurements of the experiments as input and assesses the effect of varying the velocity and number of repetitions. Finally, the model will be validated by writing MNP lines with

different deposition strategies, which are then compared to the model's predictions.

2 Methodology

First, in Section 2.1 the ADW setup is described. In Section 2.2 the different input parameters within the setup are analysed to find the key factors contributing to the SERS substrate quality. In Section 2.3 three experiments are performed to analyse the possible magnitude of the error coming from the key factors so it can be used as input for the deposition model. The deposition model is described in Section 2.4. The model is used to analyse the impact of the input parameters on the substrate quality and to find an ideal deposition strategy. This ideal strategy will be used to fabricate SERS substrates to validate the deposition model which is described in Section 2.5.

2.1 Setup

An ADW setup for SERS fabrication contains a particle generator using SAM, an Argon gas supply to carry the MNPs, a vacuum chamber, and a moving XYZ-stage to actuate the silicon substrate. The specific setup used for this study contains the VSParticle G1 nanoparticle generator. It generates between 10^9 and 10^{12} polydisperse particles per cm^3 with an average diameter of 10 nm.

The Argon gas flow is controlled by a Bronkhorst High-Tech El-Flow Prestige control valve and the pressure inside the MNP generator is limited by a variable pressure relief valve. The MNPs are transported to a vacuum chamber with a pressure of around 300 Pa where a nozzle directs the MNPs to a substrate.

The XYZ-stage consists of three SmarAct piezo stepper actuators: the SLC1750me-18 for the X-axis, the SLC1750ome-2 for the Y-axis, and the SLC1750owdme-1 for the Z-axis. The nozzle is horizontally orientated and the substrate is perpendicular to the nozzle. To keep the substrate fixed to the XYZ-stage, it is attached to a 3D-printed plate using double-sided tape. The 3D-printed plate itself is held in place by clamps which are screwed to the XYZ-stage.

The actuators are controlled using the SmarAct MCS2 controller. The controller converts the sensor outputs to position data and controls the voltage input to the actuators. The sensors are linear optical encoders and have an resolution of 1 µm. The controller allows for manual control with two joysticks. The actuators have fourteen different preset speed settings available when controlled manually. The speed settings can be altered and are defined by the piezo actuation frequency and piezo stroke. Moving at a predefined exact velocity is not possible with manual control. The controller can be connected to a computer using an USB cable to interact using SmarAct LabView, Python, or C/C++ libraries. This enables velocity control where the MCS2 controller will adjust the piezo frequency and stroke to approach a predefined velocity. Figures 3 and 4 show a photo and a schematic overview of the setup and Figures 1 and 2 show a close-up and a schematic overview of the XYZ-stage.

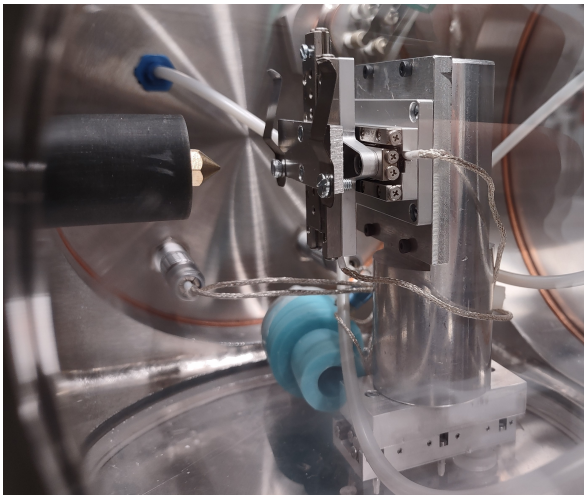

Figure 1: Photo of the XYZ-stage.

2.2 Identification of parameters contributing to the SERS substrate quality

Particle deposition is affected by a lot of different parameters within the setup. Deposition can be divided into three main components: particle generation rate, particle distribution, and XYZ-stage movement. The particle generation rate dictates how many MNPs are deposited on the silicon substrate. The particle distribution dictates how these MNPs are distributed over the substrate. The XYZ-stage movement determines how long a spot of the silicon substrate is exposed to MNP deposition.

To identify the different contributing factors to the SERS substrate quality, the three main deposition components are analysed. For each component, the input parameters that affect them are identified. For each parameter it is determined, how it affects its main deposition component

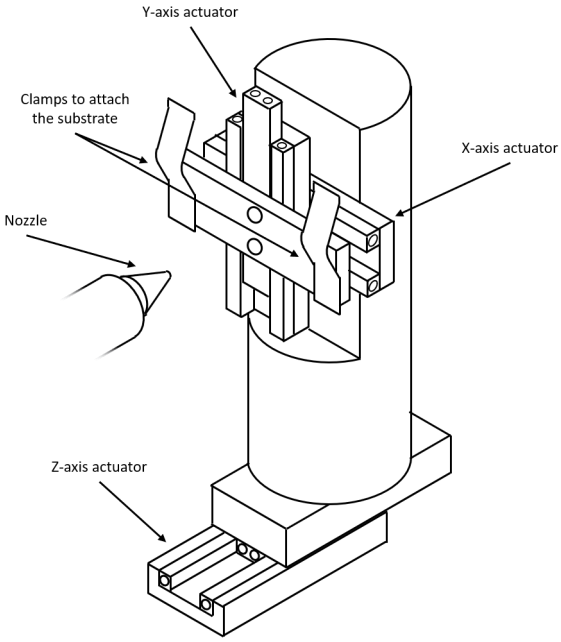

Figure 2: Schematic overview of the XYZ-stage.

and how it can be controlled by the user. Figure 5 shows each main deposition component with its corresponding parameters.

2.2.1 Particle distribution

Particle distribution determines the dispersion of MNPs across the substrate. This is affected by how much MNPs deviate from their initial trajectory after they exit the nozzle. Larger deviations result in a more spread-out distribution. The degree of deviation is affected by the Stokes number, the working distance, and the nozzle.

The Stokes number is a dimensionless number which characterises how close particles follow the flow streamlines. For a higher Stokes number, the movement of a particle is affected more by its inertia and less by flow streamlines [10]. The streamlines of the flow in the vacuum chamber will flow around the substrate so increasing the Stokes number is important to keep the MNPs on their trajectory towards the substrate. The Stokes number itself is affected by the vacuum pressure and the particle size.

A lower vacuum pressure will increase the Stokes number. The setup does not allow for control of the upstream and vacuum pressure. The vacuum pressure is around 300 Pa but can differ between sessions without having any control of it.

Particle size is affected by a lot of different parameters. The particle size can be approximated by Equation 1 which contains mass production rate $\dot{m}$, coagulation coefficient β, effective chamber volume V, material density ρ and volume flow rate Q. The mass production rate is a function of a material-dependent constant and the spark energy [11]. In practice, the particle size will be polydisperse with a lognormal distribution. Only the electrode material, the volumetric gas flow rate, spark current, and spark voltage can be controlled. The electrode material and the volumetric gas flow rate will remain constant during MNP deposition. The spark current and voltage can fluctuate during MNP deposition out of the control of the user. Some of the parameters which affect particle size and the particle size distribution are unknown.

$$d_p \approx \left(\frac{\dot{m}\beta V}{\rho \frac{\pi}{3} Q^2} \right)^{\frac{1}{3}} \tag{1}$$

The working distance is the distance from the nozzle outlet to the silicon substrate. The MNPs need to stay on their trajectory longer if the working distance is increased. The working distance remains constant during MNP deposition and can be easily controlled by using the moving XYZ-stage.

The nozzle is characterised by the nozzle type and outlet diameter. Examples of nozzle types are regular 3D printing nozzles, nozzles containing aerodynamic lenses, and sheath gas nozzles. All nozzles are available with different outlet diameters. Nozzles with sheath gas or aerodynamic lenses try to focus the MNPs to decrease particle trajectory deviations. Different nozzle types are available for the setup but in this study, only the 3D printing nozzle is used. The nozzle diameter dictates the area where MNP can exit the nozzle. A bigger diameter will increase the area where MNPs hit the substrate and thus affect the particle distribution.

2.2.2 Stage movement

The movement of the actuator directly affects how the particles are spread out along the line. If the actuator movement is not constant it can cause irregularities in the SERS substrate. The movement is defined by the operating velocity and the stage movement characteristics.

The operating velocity affects particle coverage. Higher velocities will result in less particle coverage. Different velocities can also affect the impact of irregularities in

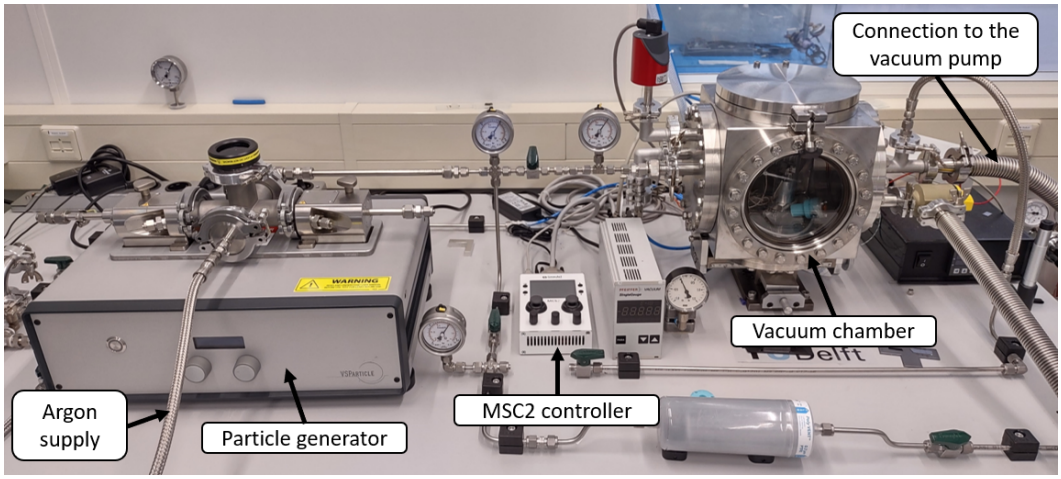

Figure 3: Photo of the ADW setup.

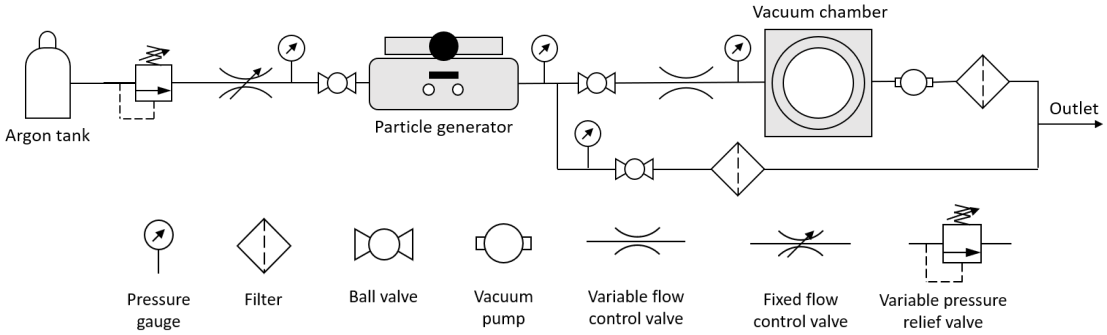

Figure 4: Schematic overview of the ADW setup.

the movement. At higher velocities the deviations from the target velocity might be smaller. The user can provide a target velocity to the XYZ-stage.

In practice it is difficult to create motion with a perfectly constant velocity. The stage movement characteristics dictate how the XYZ-stage deviates from the target velocity. Parameters affecting the movement characteristics include actuator type, control method, sensor resolution and wear. Because of the many parameters affecting the movement, it is difficult to predict the exact movement characteristics of the XYZ-stage.

2.2.3 Particle generation rate

Particle generation rate dictates how many MNPs are created. Fluctuations in the particle generation rate causes irregularities in the SERS substrate. The particle generation rate itself is dictated by the spark frequency.

The spark frequency can be calculated using Equation 2 where I is the current, C is the capacitance and V_d is the discharge voltage [9]. The discharge voltage depends on the electrode material, the pressure and the electrode gap distance. The particle generator has the current and discharge voltages as inputs. The generator will vary the electrode gap distance to achieve the target current and discharge voltage. In practice the discharge voltage is unpredictable and, therefore the spark frequency is also unpredictable. Generally the spark frequency lies between 10 and 100 Hz. The spark frequency cannot be controlled directly.

$$f = \frac{I}{CV_d} \tag{2}$$

2.3 Experiments

An experiment will be performed for each main deposition component to gain insight into the input parameters and to obtain input for the deposition model. Not all input parameters will be included in these experiments and the deposition model.

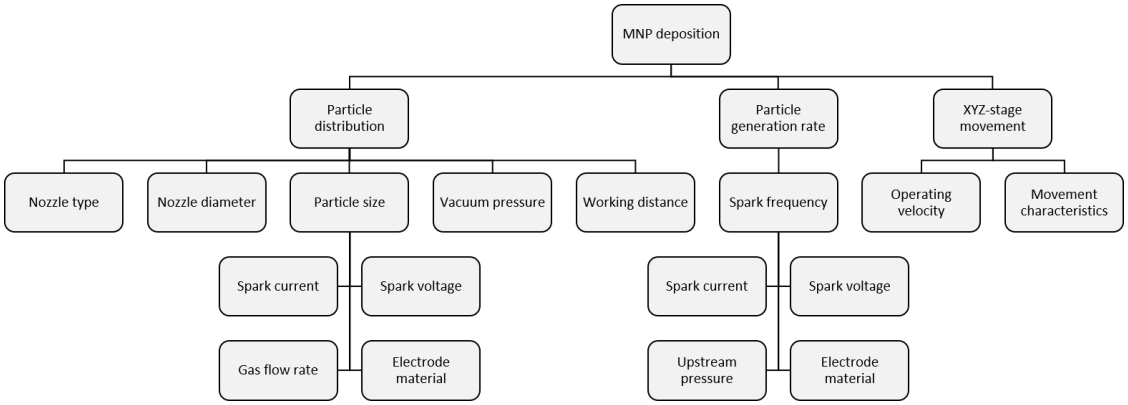

Figure 5: Categorisation of the different parameters directly affecting the particle deposition.

2.3.1 Particle distribution

MNP lines fabricated using ADW will be analysed in the experiment on particle distribution. Multiple lines will be fabricated with varying nozzle outlet diameters and varying working distances. Vacuum pressure, particle size, and nozzle type will not be included in the experiment and are assumed to be constant in the deposition model. This is done to simplify the model and to limit the input parameters. Not all parameters that affect particle size are known which is an additional reason to not include it.

Working distances of 100, 200, 300, 400, and 500 µm are combined with nozzle diameters of 200, 300, 400, and 500 µm. This results in 20 different combinations of working distance and nozzle diameter. Each combination will be fabricated twice, each on a different substrate, resulting in a total of 40 MNP lines.

The MNP line cross-section profiles are obtained to analyse particle deposition. The line profile is obtained using white light interferometry (WLI). WLI is performed with the Bruker Contour GT-K optical microscope using the 2.5X magnification lens. It has a vertical sub-nanometer resolution and a 380 nm lateral resolution. The open-source software Gwyddion is used for post-processing and to obtain the deposition profile cross-section. For each line, five cross-sections are taken.

The particle deposition distribution is assumed to be a Gaussian curve. Full-width half maximum (FWHM) is considered as the spot size, or in the case of a MNP line, the line width. FWHM is the width of the Gaussian curve at a value of half the maximum value of the curve as shown in Figure 6. FWHM is directly related to the standard deviation of a Gaussian curve following

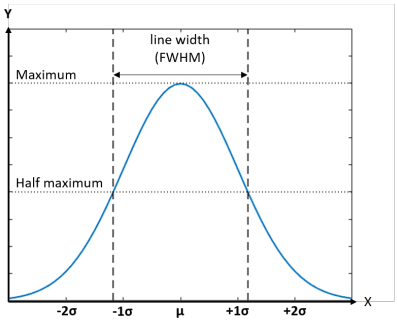

Figure 6: Schematic drawing of the full-width half maximum

Equation 3. Matlab is used to apply a Gaussian fit on the obtained cross-section data which will be used to compare the cross-sections against each other.

$$FWHM = 2\sqrt{2\ln 2}\sigma \approx 2.355\sigma \tag{3}$$

2.3.2 Stage movement

Measurements are performed to characterize the movement of the XYZ-stage used in the setup. It is possible to obtain measured position data from the controller but this is not time-stamped and it is not possible to obtain it with a fixed frequency. The controller of the actuators has a built-in sensor with a resolution of 1 µm. This is a low resolution considering the nanometre range step size of the piezo stepper. Obtaining measurements from the controller is not a reliable method to obtain data on the movement characteristics of the actuator, therefore an external sensor is used instead.

The Renishaw RLD10 fibre optic laser encoder which uses interferometry is used to perform measurements on

the actuator movement. It is a quadrature encoder and it will operate with a 80 nm resolution and a 312.5 kHz sampling rate. The XYZ-stage is raised above the vacuum chamber lid and a target mirror is attached to the stage. The laser head is targeted at the mirror to only measure the X-axis actuator movement. Velocity control by the MSC2 is used and the measured velocities range from 50 to 3000 $\mu m\,s^{-1}$. Strokes in both directions are measured. The length of the stroke varies depending on the velocity because long strokes at low velocities result in files that are too big due to the high sampling rate.

Apart from using the measured position data as input for the deposition model, the position data is also analysed to find any consistent errors in the stage movement. The mean average error (MAE) and normalised mean average error (NMAE) with respect to the target velocity are calculated to see how this specific XYZ-stage performs for different target velocities. A Fourier transform is performed on all measurements to see if there are any consistent oscillations within the stage movement. The spatial wavelengths of any found oscillations are calculated to see if these oscillations are significant compared to the spot size. Spatial wavelength can be found by using Equation 4 where v is the actuator velocity and f is the oscillation frequency. How oscillations that are deemed significant affect SERS substrate quality will also be analysed using the deposition model. To do this, position input into the model with only the isolated oscillations will be studied.

$$\lambda = \frac{v}{f} \tag{4}$$

2.3.3 Particle generation rate

To get insight into the irregularities of the particle generation rate the lines created for the nozzle diameter and working distance analysis are also analysed with regards to particle generation. For this analysis, profiles will be obtained along the MNP line instead of across. A Fourier transform analysis will be performed to see at what frequencies the fluctuations occur. The height profile will be used as input for the particle generation rate in the deposition model to test how it affects the SERS substrate quality for different XYZ-stage velocities. Similar to the tests on XYZ-stage movement isolated changes in particle generation will also be tested.

2.4 Deposition model

A particle deposition model is created to analyse the sensitivity of the SERS substrates to the different input parameters contributing to the substrate quality. It will also be used to find an ideal operating velocity for the setup used in this study, which will decrease the errors as much as possible.

A position path is provided as input to the model. The position path contains XY-coordinates which represent the movement of the XYZ-stage. On every point on this position path, the model creates a number of particles based on the particle generation rate. Positional XY-coordinates are assigned on all particles based on a Gaussian distribution. The average of the Gaussian distribution is the current position on the position profile. The standard deviation is based on the expected spot size which follows from the nozzle diameter and working distance. The total XY-plane containing particles is divided into cells of equal area resulting in a grid. Per cell, the model counts the number of particles designated to that area to obtain the predicted particle distribution. The line height is normalised because the particle size is not accounted for and the number of simulated particles is less than the actual number of particles generated. This way it is easier to compare line consistency between simulations. Figure 7 shows a schematic representation of the particle deposition model.

A number of simulations will be done with the deposition model. Fluctuations in particle generation rate and in velocity are introduced in the simulations. The velocity is constant for varying particle generation rate and the particle generation rate is constant for varying velocity. Two scenarios with varying particle generation rate are simulated. One uses the measurements from the particle generation experiment and one uses an input created in Matlab where particle generation drops are introduced at a fixed frequency. There are also two scenarios for the velocity fluctuations. One uses the measurements from the XYZ-stage experiment and one uses an input created in Matlab where velocity oscillations are introduced to an otherwise constant velocity.

The different scenarios are simulated for multiple operating velocities to test the impact of the operating velocity. The simulation sets are done for the velocities of 100 $\mu m\,s^{-1}$, 500 $\mu m\,s^{-1}$, 1000 $\mu m\,s^{-1}$, 2000 $\mu m\,s^{-1}$ and 3000 $\mu m\,s^{-1}$ and a 10 mm path is covered. The simulation set with data input obtained in the particle generation

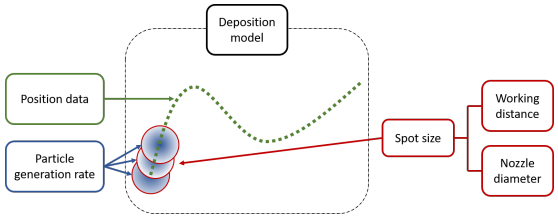

Figure 7: Schematic overview of the particle deposition model.

experiment are done for a 2.2 mm path. This is because the measurement length is limited by the white light interferometry. The simulated time remains the same within a set which results in multiple path repetitions for higher velocities. This way the amount of particles that are simulated remains the same for different velocities.

To compare the results against the baseline of numeric errors a theoretically perfect line is simulated. This line is done with one path coverage, a constant velocity of $100\,\mu m\,s^{-1}$, and a constant particle generation rate. The lines are compared based on the NMAE of the line width and the MAE of the already normalised line height.

2.5 Model validation

SERS substrates are fabricated and analysed to validate the deposition model. This will show if the model can accurately predict the line quality and if the ideal operating velocity can indeed create SERS substrates of higher quality. A total of four lines will be printed and compared. One line will be fabricated using the same method as previous research: only one path coverage and no velocity control. The other three lines will be fabricated using velocity control. Two lines will be fabricated with two different operating velocities that are predicted to result in poor SERS substrate quality. One line will be fabricated with the ideal velocity. The strategy for each line is shown in Table 1. The lines will be analysed using WLI and Raman spectroscopy.

The MNP lines are fabricated on the same silicon substrate so the fabrication process is the same for all lines. Beforehand, the silicon substrate is cleaned with acetone and isopropanol. Directly before ADW, the substrate is placed in an oxygen plasma cleaner for 30 minutes. The Argon gas flow is set at $2\,L\,min^{-1}$. The spark current is set at 5 mA and the spark voltage is set at 0.9 kV. The working distance is set at 300 µm and the nozzle diameter used is 200 µm

	Control type	**Velocity** ($\mu m\,s^{-1}$)	**Strokes**
1	Manual	100	1
2	Velocity control	100	1
3	Velocity control	2000	20
4	Velocity control	3000	30

Table 1: Line deposition strategies for final comparison

The WLI is performed with the same setup mentioned in 2.3.1. In this case, the whole MNP line will be analysed using WLI. This is done by stitching different measurements along the MNP line together. Similar to the particle generation rate measurements, three traces of the height profile will be taken along the MNP lines. Two traces right next to the MNP line will also be taken to correct for the silicon substrate profile. An average of the two substrate traces will be used to correct the MNP line profile. The MAE to the mean height will be calculated to compare the consistency of the lines.

Finally, Raman spectroscopy will be performed to analyse if a more consistent SERS substrate leads to better SERS results. The Raman spectroscopy is performed with the Horiba LabRAM HR setup equipped with an cobalt-ion laser operating at 515 nm. Rhodamine B (RhB) is used as the probe molecule. The SERS substrates are immersed in a $10^{-3}\,mol\,L^{-1}$ RhB in isopropanol solution for 24 hours to have sufficient molecules adsorbed to the substrate. The samples are washed with deionised water after the immersion. Twelve SERS measurements will be performed at equal intervals along each MNP line. The intensities of the spectra will be compared between the MNP lines. The intensities of the spectra will also be compared along the MNP line to analyze the consistency of the measurements for the same substrate. A higher quality SERS substrate should provide higher intensity measurements that are constant along the substrate.

3 Results and discussion

First, the results of the three setup experiments will be presented in Sections 3.1, 3.2, and 3.3 respectively. These results will lead to input for the deposition model simulations. The results of these simulations will be presented in Section 3.4. Finally, the results of the deposition model validation will be shown in Section 3.5.

3.1 Experiment 1: particle distribution

Figure 8 shows a WLI result with the locations where cross-section data is obtained. Figure 9 shows an example of a Gaussian fit on one of the obtained cross-sections. Figures 10 and 11 show the spot size as a function of the nozzle diameter and working distance respectively. The line follows the average spot size across all the obtained cross-sections and the error bars show the spread of the measured spot sizes.

For the working distance of 100 µm there are fewer data points because some of the lines did not have enough MNP deposition to obtain a WLI measurement. This seemed to be the result of the substrate being too close to the nozzle which hindered gas flow. The change in gas flow resulted in inconsistencies in the particle generation rate.

The figures show that the nozzle diameter has a bigger influence on spot size than the working distance. The relation between nozzle diameter and spot size looks to be linear. There is a bigger spread in spot size for the 400 and 500 µm nozzles. The particles will exit the nozzle with a higher velocity for smaller nozzle diameters because the gas flow remains the same for all nozzle diameters. This could be the reason particles deviate from their trajectory more easily for the bigger nozzle diameters. Other factors contributing to the spread of obtained spot sizes can be the vacuum pressure and particle sizes.

The correlation between working distance and spot size is less conclusive. The spot size is increasing with working distance for the 200 and 300 µm nozzles and decreases with working distance for the 400 and 500 µm nozzles. It is expected that an increased working distance would increase the spot size because there is more time for the particles to deviate from their trajectory. There might be a correlation between the gas flow streamlines and the ratio between nozzle diameter and working distance which causes these results.

To obtain consistent SERS substrates the nozzle diameters of 200 and 300 µm seem to be the best choice as they have less spread in spot size. A working distance of at least 200 µm seems to be required to keep a consistent MNP flow.

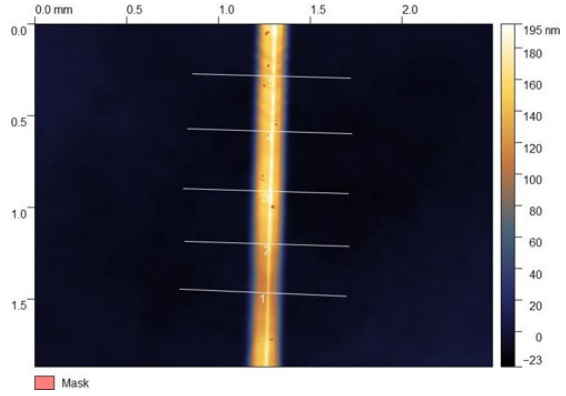

Figure 8: White light interferometry result with an example of the locations of the taken cross-sections. The line was deposited with 200 µm nozzle outlet diameter and 300 µm working distance.

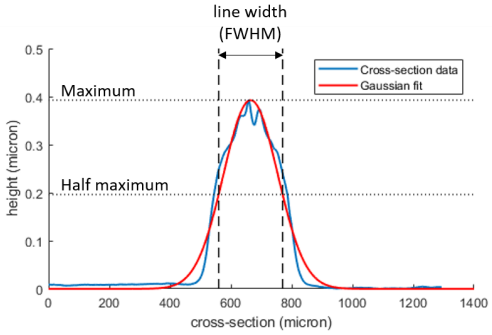

Figure 9: Cross-section data with Gaussian fit and line width definition. The line was deposited with 200 µm nozzle outlet diameter and 300 µm working distance.

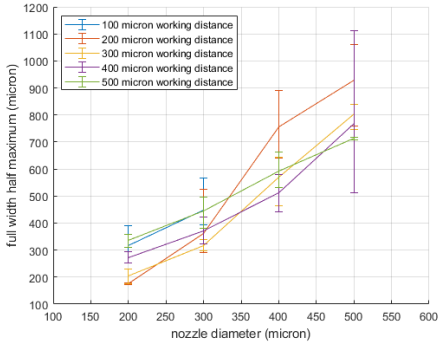

Figure 10: Average spot size for every working distance as function of the nozzle outlet diameter.

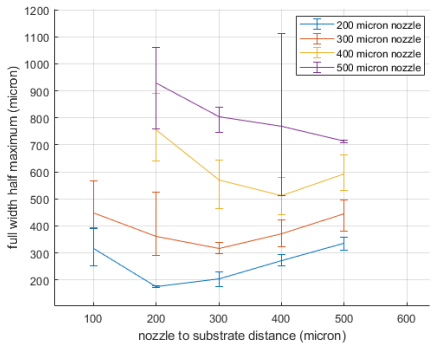

Figure 11: Average spot size for every nozzle outlet diameter as function of the working distance.

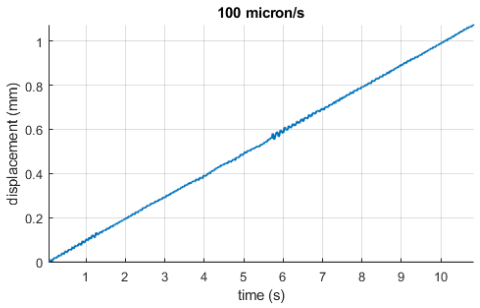

Figure 12: Zoomed in section of the measurement of a 100 µm s^{-1} velocity stroke.

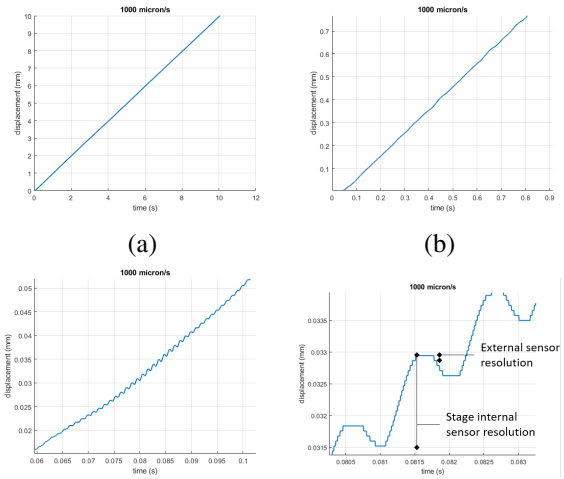

Figure 13: 1000 µm s^{-1} interferometer measurement increasingly zoomed in per subfigure.

3.2 Experiment 2: XYZ-Stage measurements

First, position measurements for three different operating velocities are shown to depict the moving stage imperfections. Figures 12, 13 and 14 show the position measurements of the XYZ-stage moving at 100 µm s^{-1}, 1000 µm s^{-1}, and 3000 µm s^{-1} respectively. Figure 12 shows a zoomed-in section of the measurement to give a better view of velocity errors. Figure 13a shows the full measurement for the 1000 µm s^{-1} velocity stroke. Figure 13b zooms in on the same measurement to show that there are oscillations within the movement. Figure 13c zooms in further to show oscillations with a higher frequency. Finally, Figure 13d shows a time period small enough so the resolution of the interferometer can be seen. The interferometer resolution and the moving stage internal encoder resolution are marked.

The figures show that over the full stroke, the average velocity matches the target velocity. All figures also show deviations from the target velocity. The deviations for the 100 µm s^{-1} velocity measurement seem to appear occasionally and then die out again. This is probably due to the controller adjusting for a velocity error. Figure 13 shows oscillations that seem to be consistent throughout the stroke. The oscillations might be a result of the frequency at which the control loop of the controller operates. The oscillations shown in Figure 13d seem to follow the resolution of the moving stage internal encoder. If these oscillations are the product of the controller and sensor characteristics, they could be predictable and therefore accounted for when deciding on operating velocity. In Figure 14 around the 4 s mark, there is a clear velocity dip. This dip occurred every time at roughly the same place on the actuator stroke for velocities higher than 2500 µm s^{-1}. This could be the result of a hardware problem at the specific location along the stroke. This hardware problem might be a defect in the encoder scale or a physical blockage resulting in higher friction.

Figures 15 and 16 show the MAE and NMAE for all position measurements relative to their target velocity. There are two measurements per velocity: one for the positive stroke and one for the negative stroke.

The MAE error increases for velocities above 2500 µm s^{-1}. This could be the result of the possible hardware problem discussed above. The NMAE tends to be higher for lower velocities. This could be the result of the 1 µm resolution of the moving stage internal encoder. At low velocities, the time between two ticks from the sensor might be too long resulting in not enough information being provided to the controller. The high absolute errors for velocities above 2500 µm s^{-1} seem to be small relative to the target velocity. Based on these measure-

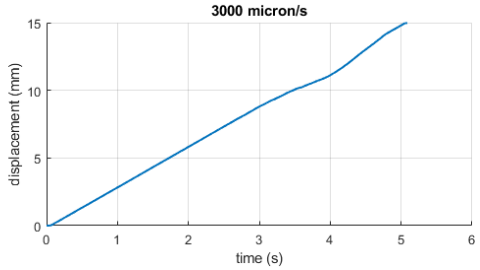

Figure 14: The measurement of a 3000 µm s^{-1} velocity stroke.

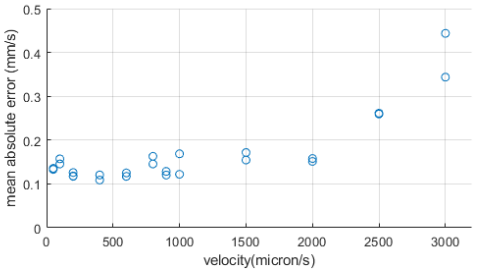

Figure 15: Mean absolute error per measured velocity.

ments the XYZ-stage seems to be operating optimally at velocities between 1000 µm s^{-1} and 2000 µm s^{-1}.

The results of the Fourier analysis are shown to get a better insight into the oscillations appearing consistently through the position measurements. Figure 17 shows how many times a peak at a certain frequency occurred in the Fourier transforms of all 26 measurements. Note that this figure does not show a Fourier transform by itself. The figure shows that at for example 48 Hz a peak occurred in the Fourier transform of 19 of the 26 measurements. The frequencies that occurred most are marked. Figure 18 shows the amplitudes of the marked oscillations as a function of the velocity. Figure 19 shows the spatial frequencies corresponding to the marked oscillation frequencies as a function of stage operating

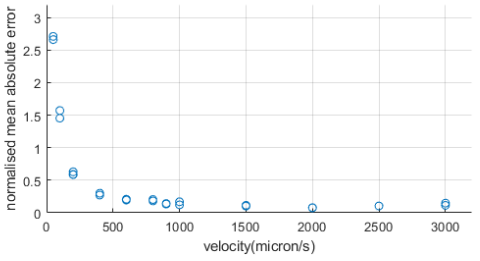

Figure 16: Normalised mean absolute error per measured velocity.

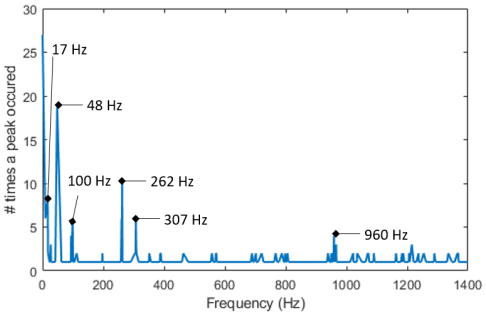

Figure 17: Number of times a frequency peak occurred in Fourier transforms of all measurements.

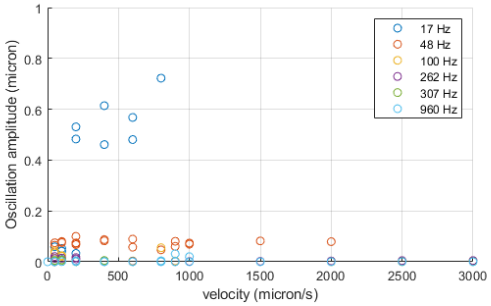

Figure 18: Amplitude of the different oscillations as function of the actuator velocity.

velocity. The dotted sections of the 17 and 48 Hz lines show where the oscillations for these frequencies have died out. The red dotted line represents 10% of the smallest spot size found in Section 3.1. Above the red dotted line, the spatial wavelength is considered to be significant compared to the spot size.

Figure 17 shows that the oscillations at 48 Hz occur in almost all measurements. This could mean that the control loop operates at 48 Hz. Figure 18 shows that the oscillations at 17 Hz have the biggest amplitude but the amplitude seems to die out after 800 µm s^{-1}. The second highest amplitude belongs to the oscillations at 48 Hz and they die out above 2000 µm s^{-1}. The other oscillations seem to be negligible compared to the 17 and 48 Hz oscillations. If the assumption that the spatial wavelength is significant above 10% of the smallest spot size is correct there are three operating windows where the oscillations would be negligible: from 0 to 400 µm s^{-1}, 800 to 1000 µm s^{-1}, and 3000 µm s^{-1} and above. To test this the 17 and 48 Hz oscillations are included in the isolated velocity deviation simulations.

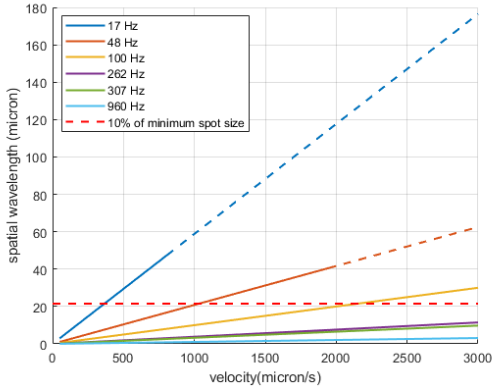

Figure 19: Spatial wavelength as a function of stage operating velocity.

3.3 Experiment 3: particle flow rate consistency

To show the possible inconsistencies in particle generation the line with the biggest height variation is shown. Figure 20b shows three traces of a height profile taken along the same MNP line. In Figure 20a the WLI measurement of this line is shown. The line is fabricated with a 200 µm nozzle diameter, a 300 µm working distance, and one 80 µm s^{-1} path coverage. The distance the actuator travels in 1 s is marked. Figure 21 shows the Fourier transform of trace 1 from Figure 20.

There are some significant drops in height along the shown line. The biggest drop appears over a period of roughly 8 s. The spark frequency of the particle generator is between 10 and 100 Hz and can be inconsistent. The particle flow will also even out in the particle generation chamber. The long drop in MNP line height could indicate that there are particle generation dropouts or that the number of particles generated per spark varies significantly.

The Fourier transform shows that the amplitudes are above 1 nm for spatial frequencies up to 10^{-2} µm^{-1}. These are deviations of 0.5 to 10% of the MNP line height which could be significant. The spatial frequency of 10^{-2} µm^{-1} corresponds with a 1.25 s period and a spatial wavelength of 100 µm. The spatial wavelength is well above 10% of the spot size which was shown in Figure 19. This indicates that the effects of particle generation are dominant over the effects of stage movement.

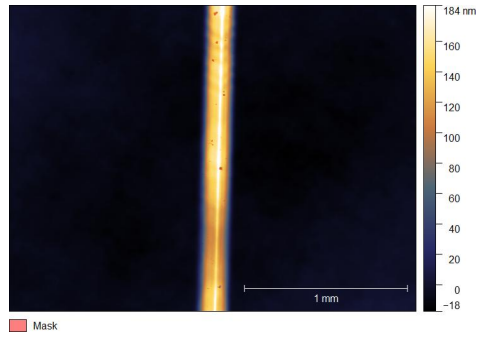

(a) WLI measurement

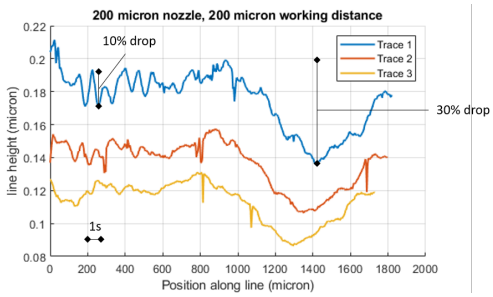

(b) Three height profile traces

Figure 20: Height profile measurements of a MNP line. The line was deposited with 200 µm nozzle outlet diameter and 300 µm working distance.

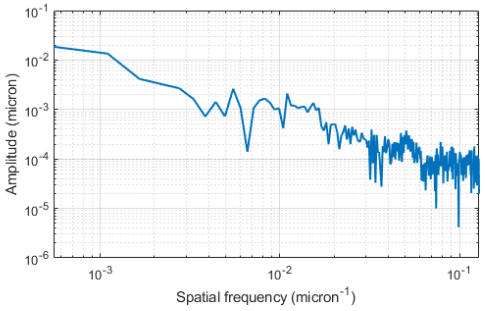

Figure 21: Fourier transform of height profile trace 1 shown in 20.

3.4 Deposition simulations

Figure 22 shows the results of the perfect line simulation. The red dots indicate the line width (FWHM). Figures 23 to 27 show the simulation results for each simulation set, with respective operating velocity indicated alongside the corresponding simulation. Figure 23 shows the simulations with isolated 17 Hz oscillations in velocity. Figure 24 shows the simulations with isolated 48 Hz oscillations in velocity. Figure 25 shows the simulations with lowered particle generation every 20 s. Figure 26 shows the simulations based on measured position data and finally, Figure 27 shows the simulations with particle generation rate data. Table 2 shows, for each simulation, the calculated NMAE of the line width and the MAE with respect to the already normalised line height.

The lines with isolated velocity oscillations seem to have no drop in quality. This is contrary to what was expected based on the spatial wavelength analysis. The position data resulted in big deviations for the 3000 µm s^{-1} simulation. This was not expected as the relative error was small. The errors in Figure 26 could be exaggerated because every back-and-forth path coverage was simulated using the exact same velocity profile. This velocity profile contained two separate measurements: one measuring a stroke in positive X-axis direction and one measuring a stroke in negative X-axis direction. Errors that occurred randomly in the stage movement were therefore present in the simulation at the same location for every path coverage. Since the error appearing for the 3000 µm s^{-1} velocity is suspected to be a hardware problem the error could actually be at the same spot for every path coverage. The big relative error at lower velocities seems to have less impact.

Table 2 shows that line width seems to be unaffected by introduced errors. Consistency of line height is affected by the introduced errors. Particle generation rate was expected to be more dominant than stage movement and this seems to be confirmed by Figures 25 and 27 and Table 2. Increased velocity seems to lower the amplitude of the MNP line height deviation. Multiple path coverages even out the particle distribution along the path and therefore seem to be a good solution for inconsistent particle generation. The MNP line simulated for 500 µm s^{-1} has five path coverages and already shows big improvements compared to one path coverage. Results from Section 3.2 did indicate that an optimal operating velocity would lie between 1000 and 2000 µm s^{-1}. Table 2 indicates that a velocity of 500 µm s^{-1} is already high enough to

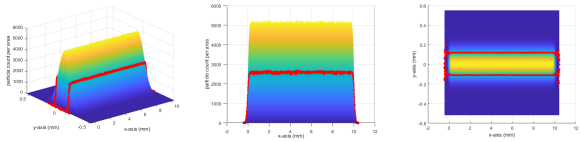

(a) 3D view (b) Side view (c) Top view

Figure 22: Perfect line simulation.

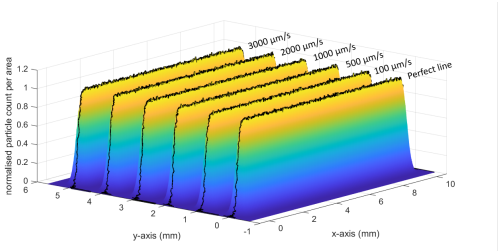

Figure 23: Simulations with introduced oscillations in velocity with a frequency of 17 Hz.

even out setup inconsistencies.

3.5 Deposition model validation

First, the height profile results are presented. Figure 28 shows the WLI results of the four MNP lines fabricated for the model validation. Figure 29 shows at which locations the height profiles were taken from the WLI data and Figure 30 shows the resulting height profiles. Figure 31 shows the height profiles that are corrected for the substrate profile. Table 3 shows the calculated MAE error compared to the average line height for both the height profiles and the substrate-corrected height profiles.

It is clear that there is a significant difference in substrate quality between the four lines. The two 100 µm s^{-1} lines both have segments where there is a clear deficit in MNP deposition. This is probably the result of particle generation dropouts as the stage movement is not expected

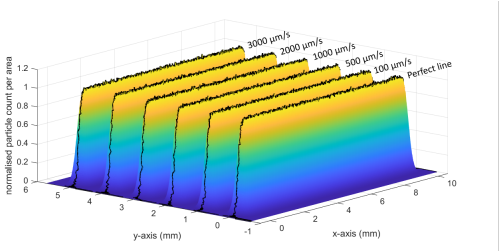

Figure 24: Simulations with introduced oscillations in velocity with a frequency of 48 Hz.

	100 µm s^{-1}		500 µm s^{-1}		1000 µm s^{-1}		2000 µm s^{-1}		3000 µm s^{-1}	
	Width error	Height error	Width error	Height error	Width error	Height error	Width error	Height error	Width error	Height error
Baseline	0.0098	0.0166	-	-	-	-	-	-	-	-
17 Hz oscillation	0.0099	0.018	0.01	0.0263	0.0101	0.0211	0.0097	0.0199	0.0097	0.0267
48 Hz oscillation	0.0096	0.0189	0.0095	0.0189	0.01	0.0192	0.0099	0.0208	0.0104	0.0222
Particle generation drops	0.0106	0.0429	0.0109	0.0242	0.0108	0.0228	0.0101	0.0291	0.0097	0.0225
Position measurements	0.0096	0.0237	0.0097	0.0208	0.0098	0.0257	0.0097	0.019	0.0099	0.0666
Particle generation data	0.0096	0.0863	0.0097	0.0295	0.0098	0.0223	0.0097	0.0237	0.0099	0.0233

Table 2: Simulation results.

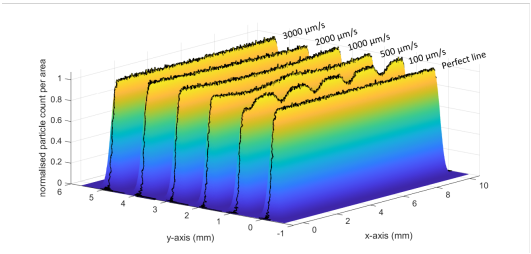

Figure 25: Simulations with introduced particle generation drops.

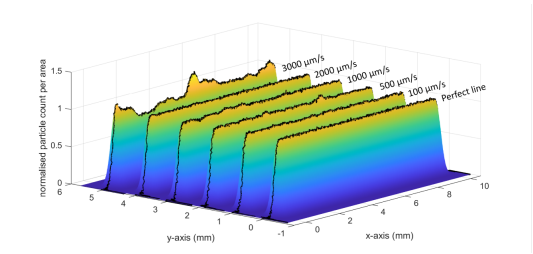

Figure 26: Simulations with data obtained in the XYZ-stage experiment.

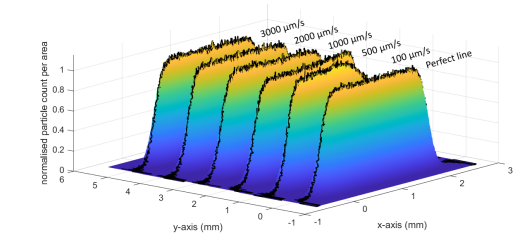

Figure 27: Simulations with data obtained in the particle generation rate experiment.

to have this big of an impact. This means that the simulations correctly showed the particle generation rate to be a dominant factor in substrate quality. Multiple path coverages and higher velocities minimised the effect of the particle rate as expected.

The 3000 µm s^{-1} line did not have the height deviations predicted by the deposition model. While the line seems a bit less consistent than the 2000 µm s^{-1} line it does not have the big deviations that were expected. Both the 2000 µm s^{-1} line and the 3000 µm s^{-1} gradually slope down. This could be the result of bad alignment of the substrate where the substrate is not perfectly perpendicular to the nozzle. A bigger distance from the nozzle to the substrate could then result in a more spread-out particle deposition and thus lower line height. This could also explain why this slope seems to be linear.

Table 3 shows that the 2000 µm s^{-1} line is the most consistent, as was predicted. The slope does distort the data as the error is calculated compared to the average height. This results in the 3000 µm s^{-1} having height errors similar to the 100 µm s^{-1} while being more consistent. The model does seem to give a decent indication of which factors are dominant in substrate quality. It also gave a decent indication of an ideal operating velocity. However, the simulation for the 3000 µm s^{-1} line did not align with expectations, as smaller line height deviations were obtained compared to what is shown in Figure 31. This could be the result of a lack of distinct measurement data for each path coverage, indicating a problem introduced by the input and not by the model.

Finally, the Raman spectroscopy results are presented. Figure 32 shows the Raman spectra of the twelve measurements for every MNP line. Figure 33 shows the Raman intensity at 1648 cm^{-1} along the MNP lines. The measurement locations are roughly indicated with the red dots and correspond with the X-axis of the graph.

The characteristic Raman peaks of RhB lie at 621 cm^{-1},

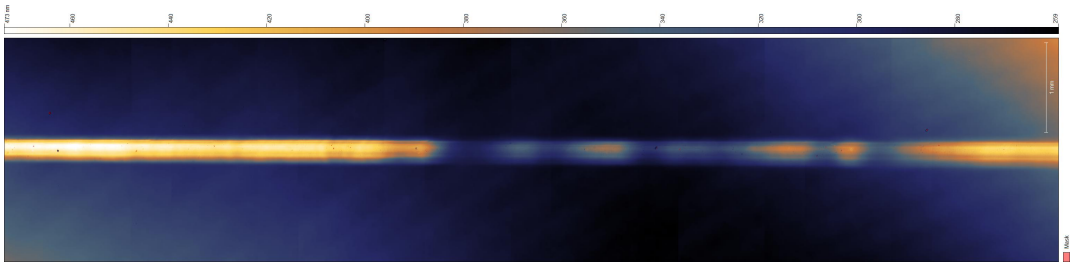

(a) manual

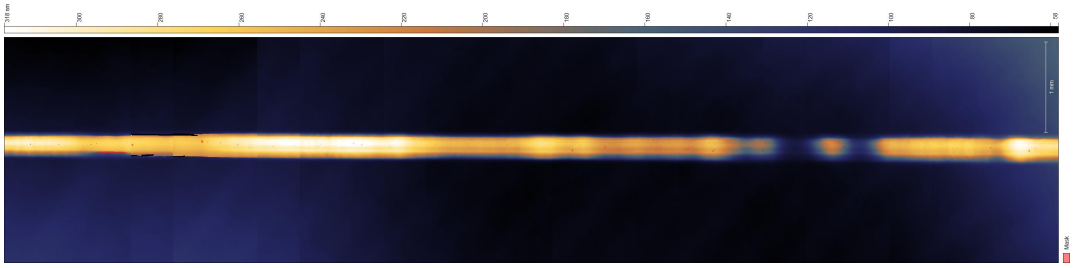

(b) $100\,\mu m\,s^{-1}$

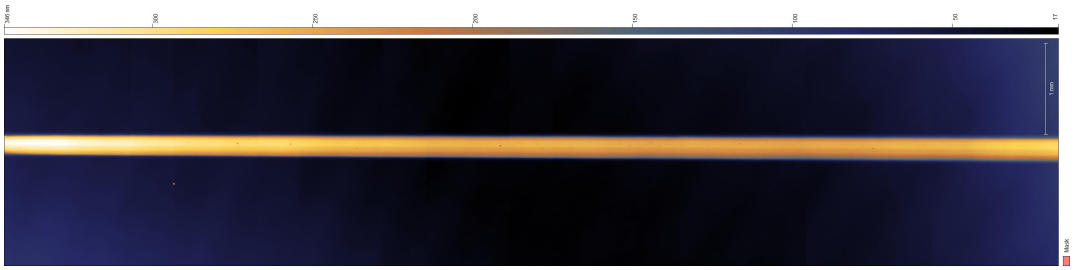

(c) $2000\,\mu m\,s^{-1}$

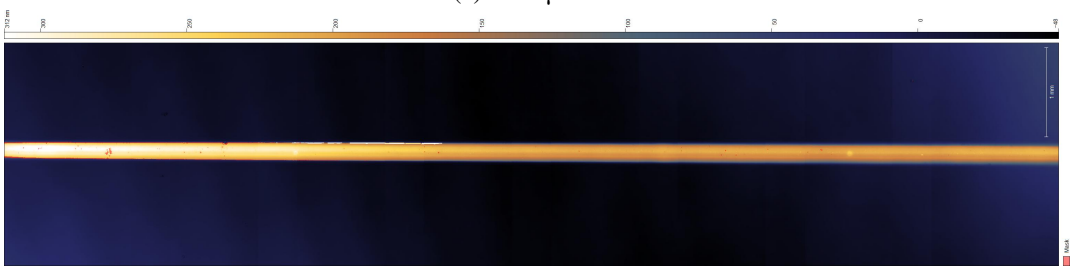

(d) $3000\,\mu m\,s^{-1}$

Figure 28: WLI results of the deposition model validation substrates.

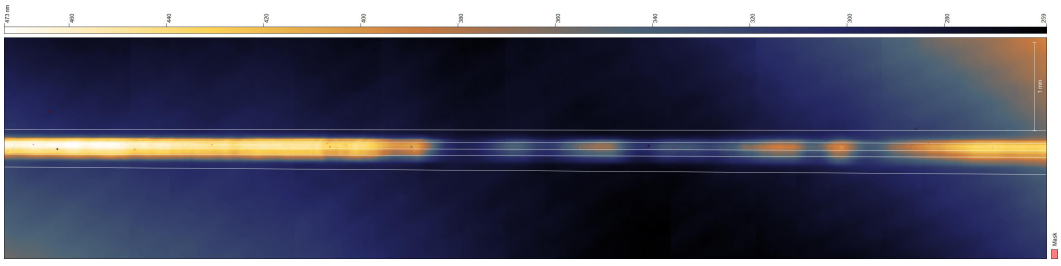

Figure 29: Example of height profile traces.

	Manual		100 µm s^{-1}		2000 µm s^{-1}		3000 µm s^{-1}	
	MAE	cMAE	MAE	cMAE	MAE	cMAE	MAE	cMAE
Trace 1	0.0402	0.0327	0.0300	0.0280	0.0235	0.0224	0.0314	0.0307
Trace 2	0.0483	0.0405	0.0323	0.0291	0.0233	0.0198	0.0338	0.0328
Trace 3	0.0460	0.0396	0.0368	0.0366	0.0234	0.0209	0.0327	0.0320

Table 3: Model validation MNP line height errors.

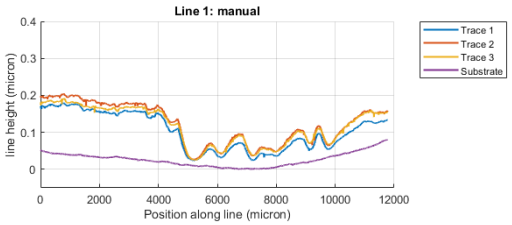

(a) manual

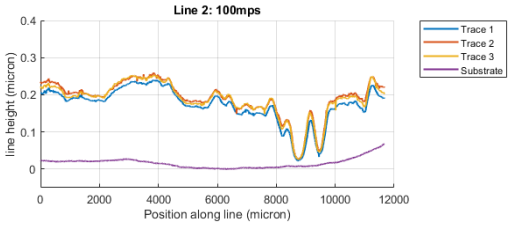

(b) 100 µm s^{-1}

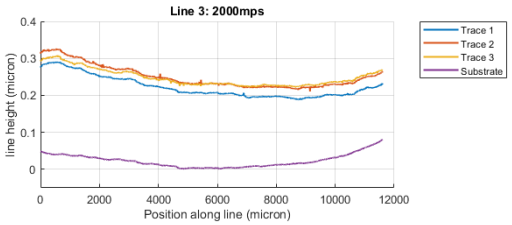

(c) 2000 µm s^{-1}

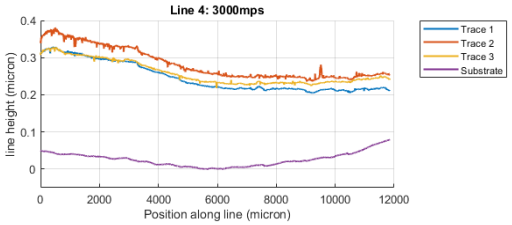

(d) 3000 µm s^{-1}

Figure 30: Line height profiles of the deposition model validation substrates.

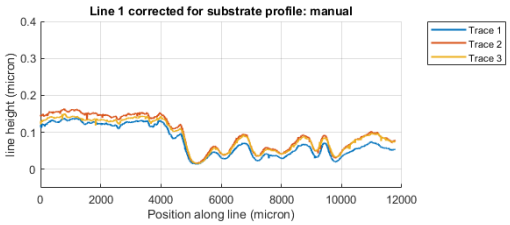

(a) manual

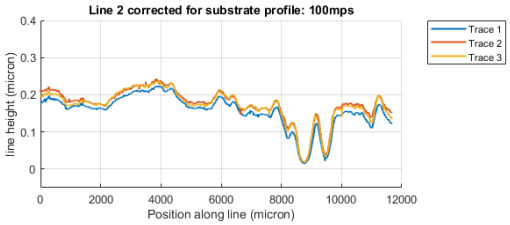

(b) 100 µm s^{-1}

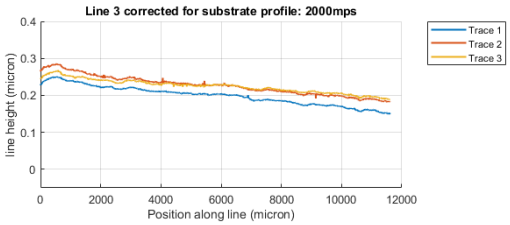

(c) 2000 µm s^{-1}

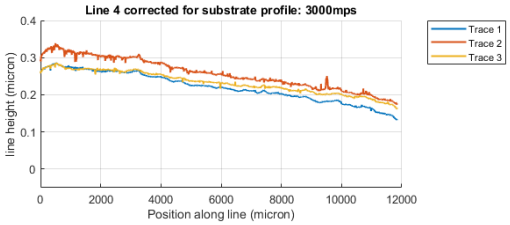

(d) 3000 µm s^{-1}

Figure 31: Line height profiles of the deposition model validation substrates that are corrected for the substrate profile.

1199 cm^{-1}, 1279 cm^{-1}, 1358 cm^{-1}, and 1648 cm^{-1}. The 621 cm^{-1} peak is not distinctively present in every measurement but the other peaks are clearly present which means RhB was successfully detected. In both Figure 32a and Figure 32d there is a measurement with only a peak present at 520 cm^{-1}. This is the characteristic peak of silicon. During the substrate preparation, the MNP lines corresponding with Figures 32a and 32d where slightly damaged while removing the substrate from the RhB solution. This caused the removal of the MNPs on small sections of the line. The measurements where the 520 cm^{-1} peak is present were taken at these damaged locations.

Figures 32 and 33 clearly show that the MNP line fabricated with an operating velocity of 2000 $\mu m\,s^{-1}$ has the most constant measurements. This in in line with the expectations based on the deposition model. Figures 32a and 32b clearly show that a MNP line with inconsistent line height also results in inconsistent Raman intensities. Figure 33 shows that lower particle coverage results in a lower Raman intensity which is expected.

The Raman intensity of the MNP line fabricated with an operating velocity of 2000 $\mu m\,s^{-1}$ is generally lower than the 100 $\mu m\,s^{-1}$ line. The MNPs are less spread out along the line fabricated at 100 $\mu m\,s^{-1}$. This could mean that at line sections with higher MNP coverage are created. These peaks could explain the high Raman intensities on a substrate that was expected to have lower quality.

4 Conclusions

The key factors contributing to SERS substrate quality within the ADW setup were identified. Measurements on these key factors were performed to serve as input for a particle deposition model. The deposition model can be used to test which factors are the dominant contributors to the substrate quality and to find an ideal operating velocity for the XYZ-stage used in the setup. The model and ideal velocity were validated by direct writing four MNP lines. These lines were compared using WLI and SERS.

It was found that the nozzle diameter and spot size have a linear correlation and the nozzle diameter seemed to be the dominant factor for the resulting spot size. The particle generation rate showed to be inconsistent and a dominant factor in SERS substrate quality. The ef-

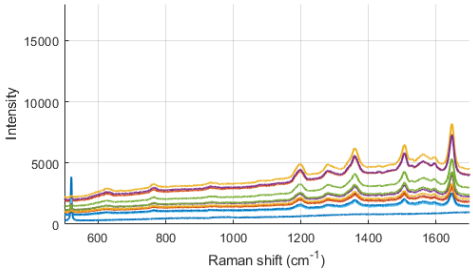

(a) manual

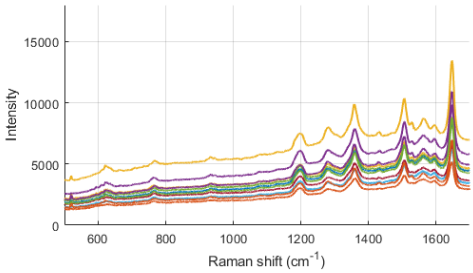

(b) 100 $\mu m\,s^{-1}$

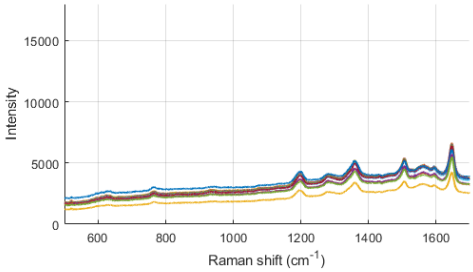

(c) 2000 $\mu m\,s^{-1}$

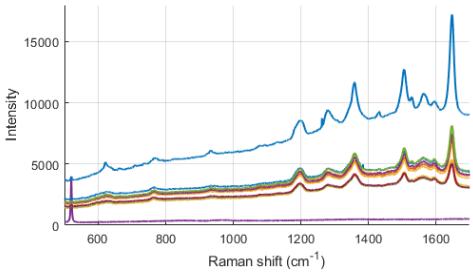

(d) 3000 $\mu m\,s^{-1}$

Figure 32: Raman spectra of the twelve measurements for each MNP line.

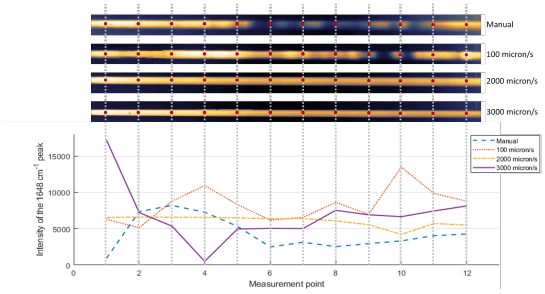

Figure 33: Raman intensity at 1648 cm^{-1} along the MNP lines. Locations of the measurements are indicated with the red dots and correspond with the X-axis of the graph.

fect of the fluctuating particle generation rate could be minimised by multiple path coverages and higher operation velocities. It was found that the XYZ-stage in the used setup operates optimally between 1000 $\mu m\,s^{-1}$ and 12 000 $\mu m\,s^{-1}$. The effect of the stage movement was however negligible compared to the particle generation rate.

The deposition model was partially successful in predicting line quality. It correctly showed particle generation rate to be the dominant factor in substrate quality. It also had a decent prediction of the ideal operating velocity. However, the simulation based on the 3000 $\mu m\,s^{-1}$ velocity data did not fit with the validation. This is considered an input problem, which indicates additional simulations with varied input data would likely lead to more conclusive results from the model. The model can be used in the future to find an ideal operating velocity and look at the effects of stage movement characteristics and particle generation fluctuations in ADW setups.

The SERS substrate fabricated with the predicted ideal operating velocity performed more consistent than SERS substrates fabricated with other operating velocities. The MNPs were more evenly spread out along the substrate and this resulted in consistent SERS measurements. The Raman intensities of the ideal substrate were not higher compared to the other substrates. The deposition model can thus be used to create more consistent SERS substrates.

Future research could look into a couple of things. Only one MNP line was fabricated using the estimated ideal operating velocity. Future work should test if this operating velocity also results in a SERS substrate that is consistent over multiple fabrications. The line simulations did not take particle size and pressure into account and assumed the particle distribution to be consistent among different uses of the setup. Future research could look at the influence of particle size and pressure on the particle distribution. Finally, simulations with more position data as input could be done. Because the available data was limited, the position data was exactly the same for multiple path coverages for a certain velocity. This could have led to exaggerated errors. More position data might improve the results of the model.

Acknowledgements

There has been quite some struggle during this research. Therefore, I want to thank Andres Hunt and Saleh Aghajani for coaching me and keeping me going. They were very patient with me and gave great feedback. I also want to thank Patrick van Holst, Gideon Emmaneel, Alex van den Bogaard, and Bradley But for their technical support.

Lastly, I want to thank my friends and family for supporting me and providing me with lots of laughs during my time as a student. I could not have done it without you. I would like to specifically mention my granddad. He passed away when I was just starting this research so he sadly cannot watch me graduate but I know he would be very proud. Opa Koos, you were a great inspiration to me!

References

[1] B. Sharma, R. R. Frontiera, A.-I. Henry, E. Ringe, and R. P. V. Duyne, "Sers: Materials, applications, and the future background and mechanism," 2012.

[2] M. Fan, G. F. Andrade, and A. G. Brolo, "A review on the fabrication of substrates for surface enhanced raman spectroscopy and their applications in analytical chemistry," pp. 7–25, 5 2011.

[3] H. Pu, W. Xiao, and D. W. Sun, "Sers-microfluidic systems: A potential platform for rapid analysis of food contaminants," pp. 114–126, 12 2017.

[4] M. M. Hassan, M. Zareef, Y. Xu, H. Li, and Q. Chen, "Sers based sensor for mycotoxins detection: Challenges and improvements," *Food Chemistry*, vol. 344, 5 2021.

[5] S. L. S. Liu, Y. B. Y. Bai, Z. C. Z. Chen, N. C. N. Chen, J. H. J. Huang, L. L. L. Li, and B. L. B. Lu, "Sers measurement of cancerous cells with optical fiber sensor," *Chinese Optics Letters*, vol. 12, pp. S23 002–323 004, 2014.

[6] H. T. Beier, C. B. Cowan, I. H. Chou, J. Pallikal, J. E. Henry, M. E. Benford, J. B. Jackson, T. A. Good, and G. L. CotÃ©, "Application of surface-enhanced raman spectroscopy for detection of beta amyloid using nanoshells," *Plasmonics*, vol. 2, pp. 55–64, 6 2007.

[7] S. Aghajani, A. Accardo, and M. Tichem, "Aerosol direct writing and thermal tuning of copper nanoparticle patterns as surface-enhanced raman scattering sensors," *ACS Applied Nano Materials*, vol. 3, pp. 5665–5675, 6 2020.

[8] ——, "Tunable photoluminescence and sers behaviour of additively manufactured au nanoparticle patterns," *RSC Advances*, vol. 11, pp. 16 849–16 859, 4 2021.

[9] N. S. Tabrizi, M. Ullmann, V. A. Vons, U. Lafont, and A. Schmidt-Ott, "Generation of nanoparticles by spark discharge," *Journal of Nanoparticle Research*, vol. 11, pp. 315–332, 2 2009.

[10] S. Aghajani, A. Accardo, and M. Tichem, "Process and nozzle design for high-resolution dry aerosol direct writing (dadw) of sub-100 nm nanoparticles," *Additive Manufacturing*, vol. 54, 6 2022.

[11] J. Feng, G. Biskos, and A. Schmidt-Ott, "Toward industrial scale synthesis of ultrapure singlet nanoparticles with controllable sizes in a continuous gas-phase process," *Scientific Reports*, vol. 5, 10 2015.

Additional resources

Additional resources containing all measurement data, Matlab scripts, and Labview VI's are available. A guide on how the additional resources are organised is shown below.